Deformation Coupled to Director Rotation in Swollen Nematic Elastomers under Electric Fields

Kenji Urayama,* Seiji Honda, and Toshikazu Takigawa

Department of Materials Chemistry, Kyoto University, Kyoto 615-8510, Japan

Received December 28, 2005; Revised Manuscript Received January 16, 2006

ABSTRACT: Swollen nematic elastomers unconstrained by electrodes exhibit macroscopic deformation as well as an almost full (90°) rotation of director in fast response to sufficiently high electric fields normal to the initial director. The deformation is strongly coupled to the director rotation: The deformation takes place dominantly in the plane where the director rotates whereas almost no dimensional variation occurs in the direction irrelevant to the director rotation. There exists a threshold for the onset of director rotation which is determined by field rather than voltage. The constraint by electrodes prohibiting strain along the field axis strongly suppresses the director reorientation and also significantly increases the threshold field. As the cross-linking density decreases, the electrooptical and electromechanical effects become larger and the threshold decreases. The compressive strain along the initial director axis linearly varies with $\sin^2 \theta$ (θ: rotation angle of director) in good agreement with the prediction of the soft deformation theory for thin films.

Introduction

Liquid crystal elastomers (LCE) exhibit interesting properties stemming from the hybrid characters of elastomers and liquid crystals.[1] A marked characteristic of LCE is that the molecular orientation of the constituent mesogens is coupled to the macroscopic deformation and vice versa. For instance, the imposed strain perpendicular to the initial director can drive a 90° switching of the director in LCE.[2−5] In the mechanical stretching, the globally uniform shear deformation is impossible because of the clamps holding the sample from both ends. This mechanical constraint yields the nonuniform stress (strain) field in the process of the director rotation, leading to an inhomogeneous microstructure observable as a characteristic striped pattern of the director orientation.[3−7]

Electric fields have also been employed to drive the director reorientation in LCE. The LCE swollen by low molecular mass liquid crystals (nematic gels) were used as the samples[8−19] because unrealistic high fields are needed to induce a finite rotation of director in dry LCE, owing to the high elastic modulus. In the previous communication,[18] we demonstrated that the sufficiently high electric fields normal to the initial director achieve almost full (90°) rotation of director in nematic gels which are unconstrained by the electrodes. Of importance is that the simultaneous deformation takes place dominantly in the plane regarding the director rotation: The dimension along the initial director is reduced while almost no dimensional change occurs in the direction independent of the director rotation. In addition, the induced director reorientation and deformation are globally uniform since the electrically driven director switching does not need the clamping of gels: No inhomogeneous microstructure like stripe domains formed in mechanically induced director switching was observed.[18] The electric field response of nematic gels in unconstrained geometry provides an important and unambiguous basis to elucidate the mechanism of the deformation coupled to the director rotation. The deformation induced by director rotation in LCE was theoretically discussed as a function of rotation angle on the basis of soft elasticity concept.[1,20,21] The anisotropic deformation observed[18] is qualitatively similar to the theoretical picture, but the quantitative comparison has not yet been done.

The fast response of nematic gels to electric fields also attracts much attention from the viewpoint of the application to soft actuators. The direct coupling of electric fields to mesogen alignment yields a much faster actuation of LCE in comparison with the electrically driven polyelectrolyte gels governed by ionic diffusion.[22] In addition, the direction of the electrically driven stretching of LCE is controllable by the signs of dielectric anisotropy of the constituent nematogens: The dielectrically positive or negative nematic gels are stretched in the direction parallel or perpendicular to the field axis, respectively.[17] Also, the electrical deformation of monodomain nematic gels with global director accompanies a large change in birefringence as a result of director rotation. The electromechanical responses with the electrooptical effects in LCE are expected to yield interesting new applications.

In the present study, we study the details of the deformation coupled to the director rotation in nematic gels under electric fields. We investigate the effects of cross-linking density on the electric field response and also show how strongly the mechanical constraints from electrodes suppress the director realignment. We elucidate the correlation between the rotation angle of director and the dimensional changes and quantitatively compare it with the theoretical picture of macroscopic soft deformation.

Experiment

Samples. Side-chain nematic networks with global uniaxial (homogeneous) orientation were prepared by the method described in ref 23. The photopolymerization of the reactive mesogenic monomer MP (Figure 1) in the globally aligned state was carried out in a glass cell whose surface was coated by uniaxially rubbed polyimide layer. 1,6-Hexanediol diacrylate and the low molecular mass liquid crystal 4-*n*-hexyloxy-4′-cyanobiphenyl were used as cross-linker and nonreactive miscible solvent, respectively. The nonreactive nematic solvent was mixed with the reactive monomer to broaden the temperature range of nematic phase, and the mixing molar ratio was 1:1. Irgacure 784 was employed as photoinitiator. The photopolymerization was performed by the irradiation of visible

* To whom correspondence should be addressed. E-mail: urayama@rheogate.polym.kyoto-u.ac.jp.

10.1021/ma052762q CCC: $33.50
Published on Web 02/04/2006

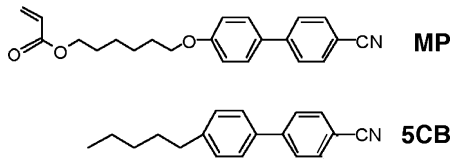

Figure 1. Molecular structures of employed reactive mesogenic monomer and nematic solvent.

Table 1. Sample Characteristics

C_x (mol %)	d_g^0 (μm)	d_p (μm)	d_t (μm)	Q	$E_{c,g}$ (MV m^{-1})	α	k
3	26	20	40	5.5	0.58	1.13	1.23
7	34	25	40	4.1	0.62	1.25	1.13
14	23	25	40	2.0	0.82	1.51	1.06

light (with wavelength of 526 nm) at a temperature lower than the nematic−isotropic transition temperature by 5 °C. The gap of the cells for the sample preparation (d_p) was 20, 25, or 50 μm.

The samples with differing cross-linking densities were prepared by varying the cross-linker concentrations in the feed (C_x). After polymerization, the slide glasses were carefully removed from the gel films, and the gel films were allowed to swell in dichloromethane to wash out the nematic solvent and unreacted materials. The swollen gels were deswollen in methanol. After drying, the networks were fully swollen in the nematic solvent 4-*n*-pentyl-4′-cyanobiphenyl (5CB, Figure 1). The initial swelling temperature was 80 °C in the isotropic phase of the gel, and thereafter the swelling was equilibrated at 25 °C in the nematic state. A monodomain nematic texture in the swollen networks was confirmed by polarizing microscopy. In the swollen state, the network and solvent form a single nematic phase without microphase separation. As is evident from the molecular structures of MP and 5CB, the nematic gels are dielectrically positive.

The degree of anisotropy in swelling (α) was evaluated by

$$\alpha = \lambda_{||}/\lambda_{\perp} \tag{1}$$

where $\lambda_{||}$ and $\lambda_{\perp}$ are the principal ratios parallel and normal to the director, respectively. The ratios $\lambda_{||}$ and $\lambda_{\perp}$ are defined as the dimensional ratios in the swollen and dry states: $\lambda_{||} = b_{||}/b_{||,\mathrm{dry}}{}^{\mathrm{I}}$ and $\lambda_{\perp} = b_{\perp}/b_{\perp,\mathrm{dry}}{}^{\mathrm{I}}$ where $b_{\mathrm{dry}}{}^{\mathrm{I}}$ is the dimension in the dry, isotropic state. The degree of swelling (Q), i.e., the volume ratio in the dry and swollen states, is calculated by $Q = \lambda_{||}\,\lambda_{\perp}{}^2$ assuming uniaxial orientation. Table 1 tabulates the characteristics of the samples including the film thickness in the swollen state (d_g^0).

Measurements. The schematic of the experimental setup is shown in Figure 2. All measurements were carried out at 25 °C. The fully swollen gels were placed between the two transparent glass plates with indium−tin oxide (ITO) electrodes. The gap between the electrodes (d_t) was adjusted by the spacers to be larger than d_g^0 so that the gels could be unconstrained by the electrodes. The constrained geometry where the gel was effectively sandwiched by the electrodes ($d_t = d_g^0$) was also employed for comparison. In the constrained geometry, no distortion along the field direction was allowed.

The cells were filled with transparent silicone oil, which is a nonsolvent for the gels. The sinusoidal electric fields were applied in the *z*-direction normal to the initial director (*x*-direction) of the gels using a function generator NF WF1943 and a high-voltage amplifier Kepco BOP1000M. The voltage amplitude (V_0) was stepwise increased up to 750 V. The employed frequency was 1 kHz.

The electrooptical effects were studied by measuring the intensity of transmitted light (I) through crossed polarizers with the sample cells using a He−Ne laser (λ = 633 nm). The initial director of the gels was at an angle of 45° relative to the optical axes of the crossed polarizers. The effective optical birefringence (Δn_{eff}: $\Delta n_{\mathrm{eff}} = n_x - n_y$ where n_i is the principal refractive index in the i-direction) was evaluated as a function of V_0 from the familiar relation $I/I_{\max} = \sin^2(\pi d_g \Delta n_{\mathrm{eff}}/\lambda)$ where d_g is the optically effective film thickness. The value of d_g at each V_0 was calculated with the strains in *x*- and *y*-directions assuming the volume conservation in the way described later.

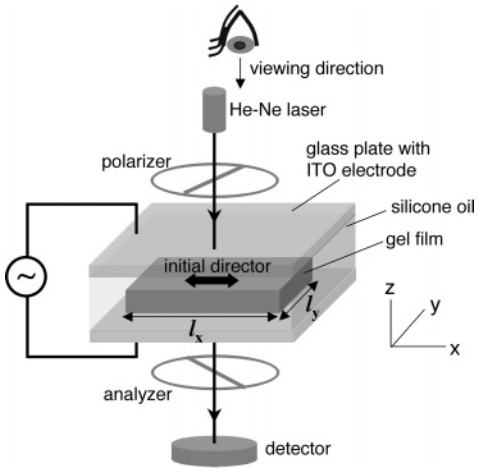

Figure 2. Schematic of the experimental setup.

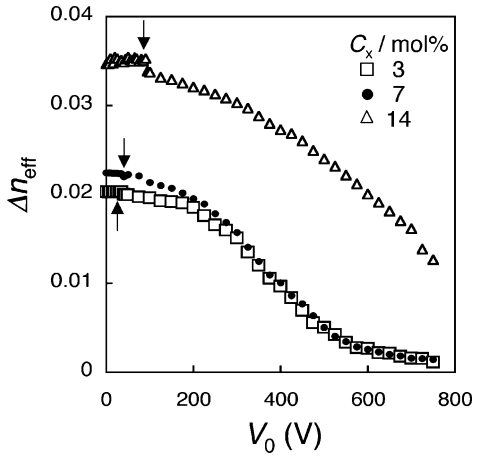

Figure 3. Effective birefringence Δn_{eff} as a function of V_0 for the nematic gels with differing C_x. The arrows indicate the threshold voltage amplitudes to yield a finite change in Δn_{eff}. The data for the gel of C_x = 7 mol % were reproduced from ref 18.

In a separate experiment, the electrically driven deformation of the gels was observed with an optical microscope Nikon E600POL. Both samples for electromechanical and electrooptical measurements were cut out from the same gel film. Rectangular films with width and length of ca. 2 mm were used in the electromechanical measurements. The dimensions of the gels in *x*- and *y*-directions were measured as a function of V_0. The strain in each direction (γ_i) were evaluated by

$$\gamma_i = (l_i - l_{i0})/l_{i0} \tag{2}$$

where l and l_0 are the dimensions in the deformed and undeformed states, respectively. The measurements of Δn_{eff} and γ at each V_0 were made about 30 s after the application of the field. This time interval is enough long to achieve the stationary state because the time required to reach the stationary value in light transmittance was ca. 5 ms.[18]

Results and Discussion

Electrooptical and Electromechanical Effects. Figure 3 displays the V_0 dependence of Δn_{eff} for the nematic gels with differing C_x in the unconstrained geometry. An increase in V_0 yields a decrease in Δn_{eff}, i.e., the growth of director reorientation along the field axis (*z*-direction). The $\Delta n_{\mathrm{eff}}-V_0$ relation is

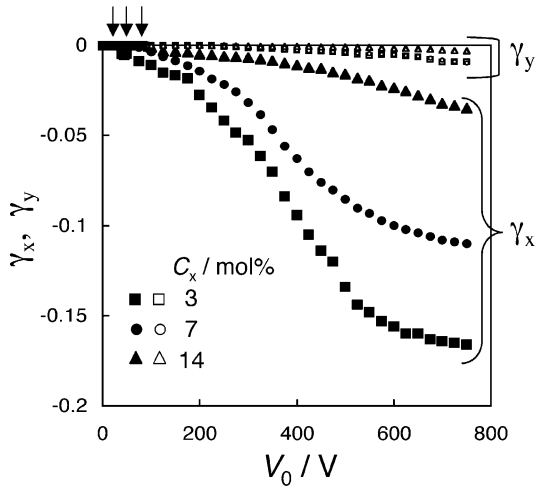

Figure 4. Strains γ_x and γ_y as a function of V_0 for the nematic gels with differing C_x. The arrows indicate the threshold voltage amplitudes to yield a finite strain. The data for the gel of $C_x = 7$ mol % were reproduced from ref 18.

reversible when repeating the application and removal of electric fields. Of importance is that Δn_{eff} for the gels with $C_x \leq 7$ mol % decreases down to almost zero (ca. 5% of the initial values) at sufficiently high V_0, indicating that the high fields achieve almost full (90°) rotation of the director. A residual (nonzero) value of Δn_{eff} at high fields may imply the presence of the surface layer where the initial nematogen alignment is immobilized by anchoring effects. For the gel of $C_x = 14$ mol %, Δn_{eff} does not show the saturation in the high V_0 region, and the minimum value still remains ca. 30% of the initial value, indicating that the high modulus acts as a resistance for the director rotation. As seen in Figure 3 and Table 1, the initial value of Δn_{eff} at $V_0 = 0$ as well as the degree of anisotropy in swelling (α) increases with C_x, showing that the global nematic order becomes larger as C_x increases. This is because the orientational order of mesogenic molecules before cross-linking is more effectively maintained in the networks upon the cross-linking reaction as C_x increases. In addition, a large swelling of the networks with low C_x acts to reduce the global nematic order before swelling.

The amplitude V_0 in the figure is the apparent voltage amplitude acting on the cell composed of the gel and silicone oil layers. A care should be taken when comparing the responses in different samples at each V_0. The voltage effectively acting on the gel depends on the thickness and effective dielectric constant of each layer. The effective dielectric constant of the gel, however, also alters with the rotation angle of director, which practically prevents from calculating the voltage acting on the gel at each V_0. Thus, we employ V_0 to display the electric field responses of the gels unless specified otherwise.

Figure 4 illustrates the strains γ_i ($i = x, y$) as a function of V_0 for the gels with differing C_x in the unconstrained state. The induced deformation is obviously anisotropic, and the dimensional variation takes place dominantly in the $x-z$ plane where the director reorientation occurs: The gels are compressed along the initial director axis (x-direction), while almost no dimensional change is present in y-direction even at high fields. The strain along the field axis (z-direction) was not directly measured because of the difficulty to detect small thickness changes in the thin films. The strains in z-direction, however, are certainly elongational (positive) because the gels are substantially incompressible like cross-linked rubbers. In addition, a direct measurement of γ_z using the cylindrical gels with positive dielectric anisotropy proved that γ_z is positive;[17] i.e., the gels are stretched along the field direction, owing to the electrical nematogen orientation. In the calculation of Δn_{eff}, the optically effective thickness (d_g) under electric fields was estimated using $d_g/d_g^0 \approx [(1 + \gamma_x)(1 + \gamma_y)]^{-1}$ on the basis of the volume constancy.

The deformation increases as C_x decreases (i.e., the modulus becomes smaller). In the case of $C_x = 3$ mol %, $|\gamma_x|$ reaches ca. 17% at the maximum V_0. An increase in C_x (i.e., modulus) suppresses the electrical deformation as well as the electrooptical effect. It should also be noticed in Figures 3 and 4 that the thresholds (V_c) to yield finite optical and mechanical responses are present. The values of V_c for each response are almost identical, and V_c depends on C_x. The discussion about the threshold is given in the next section.

Part a of Figure 5 depicts the relation between normalized values of γ_x and the change in Δn_{eff} ($\delta n_{\text{eff}} = \Delta n_{\text{eff}}^0 - \Delta n_{\text{eff}}$). Each quantity normalized by the value at the maximum V_0 varies from zero to unity. For all samples, the relation is well represented by a straight line with the slope of unity, indicating that γ_x strongly correlates with the change in birefringence. The result further supports that the deformation is strongly coupled to the director rotation. The deformation induced by the full (90°) rotation of director is schematically shown in Figure 5b.

Determinant of Threshold. The thresholds for the onset of director rotation in the gels with differing thicknesses but with identical C_x have been studied to elucidate which of electric field or voltage is the determinant of threshold. Figure 6 shows Δn_{eff} in the low V_0 region for the gels of $C_x = 14$ mol % with $d_g^0 = 23$ and 47 μm. The thresholds are clearly observed for both cells. The cells are composed of the two layers (gel and silicone oil) differing in thickness and dielectric constant. From the threshold amplitude for the cell (V_c), the corresponding voltage ($V_{c,g}$) and field strength ($E_{c,g}$) acting on the gels are calculated by

$$V_{c,g} = \frac{\epsilon_s d_g^0 V_c}{\epsilon_s d_g^0 + \epsilon_g (d_t - d_g^0)} \tag{3a}$$

$$E_{c,g} = \frac{V_{c,g}}{d_g^0} \tag{3b}$$

where ϵ_g and ϵ_s are the dielectric constants for the gels along the field axis and silicone oil. For simplicity, we assume no pretilting of nematogens in the initial state and approximate ϵ_g by the dielectric constant normal to the long axis of 5CB. The calculated values of $V_{c,g}$ and $E_{c,g}$ are $V_{c,g} = 2.1 \times 10^1$ V, $E_{c,g} = 8.2 \times 10^{-1}$ MV m^{-1} for $d_g^0 = 23$ μm and $V_{c,g} = 4.7 \times 10^1$ V, $E_{c,g} = 9.5 \times 10^{-1}$ MV m^{-1} for $d_g^0 = 47$ μm. The close values of $E_{c,g}$ but the largely different values of $V_{c,g}$ for the two samples indicate that the threshold is determined by field rather than voltage. The similar result was obtained in the studies on the electrooptical response of nematic gels in the constrained geometry of $\gamma_z = 0$.[12,13,16] The small difference in $E_{c,g}$ of the two samples is mainly due to an inevitable finite difference in the degree of initial orientation which is recognizable in the different initial values of Δn_{eff}: The anchoring force of the rubbed layers inducing a homogeneous nematogen alignment weakens as the cell gap increases. The threshold governed by field is in contrast to that determined by voltage in the Fredericks transition of conventional nematogens. This results from the different anchoring origins in usual nematogens and nematic gels, since they are substantially liquids and solids, respectively.

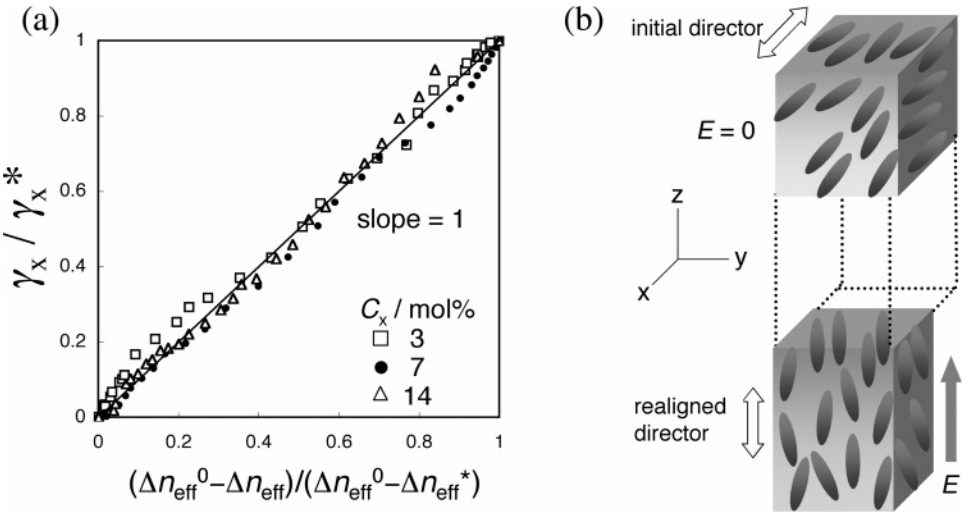

Figure 5. (a) Correlation between the reduced values of $\delta\Delta n_{eff}$ and γ_x for the nematic gels with differing C_x. The data of $\delta\Delta n_{eff}$ and γ_x are reduced using the values at the maximum V_0 (Δn_{eff}* and γ_x*). (b) Schematics for the nematic gels in the two extreme states of $\theta = 0°$ and 90°.

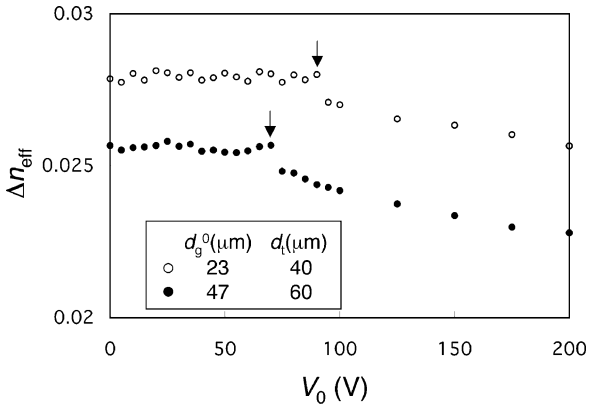

Figure 6. Effective birefringence Δn_{eff} in the low V_0 region for the nematic gels of $C_x = 14$ mol % with $d_g^0 = 23$ μm ($d_t = 40$ μm) and $d_g^0 = 47$ μm ($d_t = 60$ μm). The arrows indicate the threshold voltage amplitudes for the onset of a change in Δn_{eff}.

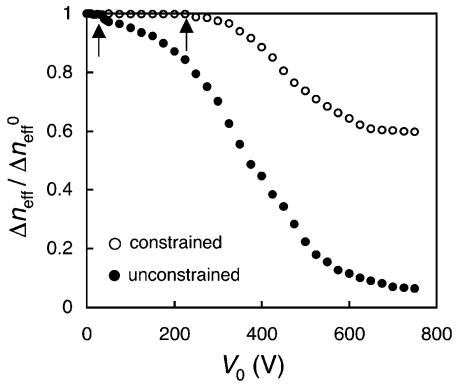

Figure 7. Effective birefringence Δn_{eff} as a function of V_0 for the nematic gels of $C_x = 7$ mol % in the unconstrained and constrained states. In the constrained state, the strain in the field direction is strictly prohibited. The data are reduced by the initial value of Δn_{eff} at $V_0 = 0$. The arrows indicate the threshold voltage amplitudes for the onset of a change in Δn_{eff}. The data for the unconstrained gel were reproduced from ref 18.

The anchoring effect in usual nematogens stems only from the surface of electrodes (substrates), which causes a large distribution of the tilt angles of nematogens with the maximum at the middle of the layer under electric fields. By contrast, the anchoring effect in the gels originates from the gel matrix, and the resultant anchoring force is primarily affected by the modulus governing rubber elasticity: As seen in Table 1, $E_{c,g}$ increases with C_x. A simple argument using the balance of dielectric and elastic energies shows $G \approx \epsilon_0 \Delta\epsilon E_{c,g}^2$ for the onset of director response, where ϵ_0, G, and $\Delta\epsilon$ are the dielectric constant of vacuum, shear modulus, and dielectric anisotropy of the materials, respectively.[24] This equation with the data of $E_{c,g}$ and $\Delta\epsilon$ for 5CB yields the values of G less than 10^2 Pa for all samples examined here. These values of G are too small compared to the typical values of G (on the order of 10^3 or 10^4) for the swollen gels with the similar C_x and Q. In other words, the thresholds observed are much lower than those expected from the typical modulus of the gels with similar characteristics. A soft elasticity concept argues that the full director rotation costs no energy in ideal LCE with neither anchoring effect nor chain interaction such as entanglement effects.[1,24−26] In the experiments, a finite threshold is present, and a high external field is required to achieve 90° rotation of director. These observations indicate that the real systems are not purely "soft", but the unexpectedly small threshold in the experiment may imply that the real systems have a "soft" character to some extent (what has been called "semisoft"[1]). Systematic data of $E_{c,g}$ and G are needed to discuss the issue of "softness" more quantitatively. The mechanical measurements of the thin soft gel films are not straightforward at present.

Effect of Mechanical Constraint by Electrodes. Figure 7 displays the comparison of electrooptical effects of the gel of $C_x = 7$ mol % in the constrained and unconstrained states. In the constrained state, the strain in the field direction was strictly prohibited ($\gamma_z = 0$), while care was taken to facilitate the deformation in x- and y-directions at the electrode surfaces by lubricating with silicone oil. In the constrained geometry, the decrease in Δn_{eff} saturates at high fields, but the total drop from the initial value is only 40%. This is much smaller than ca. 95% drop in Δn_{eff} at high fields in the unconstrained state. In addition, the threshold field in the constrained state ($E_{c,g} = 6.3$ MV/m) is about 1 order of magnitude larger than $E_{c,g} = 0.62$ MV/m in the unconstrained state. These results clearly demonstrate that the geometry prohibiting the strain along the field axis strongly suppresses the director reorientation. The suppression effect of the constrained geometry on the director rotation in LCE was theoretically discussed in ref 24.

In the constrained geometry, a nonuniform deformation was observed under electric fields. Almost no deformation takes place in y-direction as in the unconstrained case. Meanwhile,

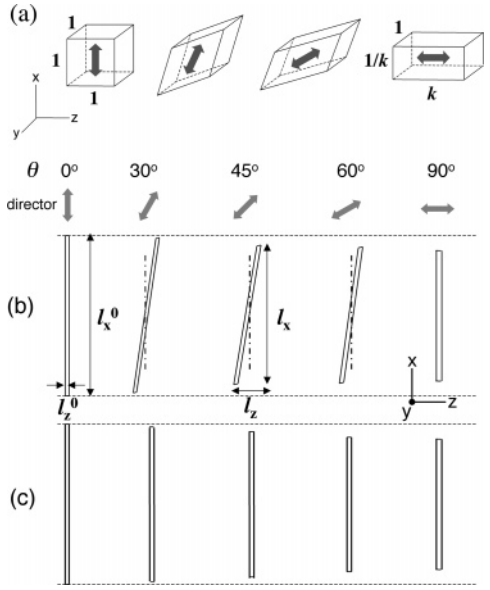

Figure 8. (a) Deformation of small volume elements with anisotropy $k = 1.5$ on the basis of eq 4. The arrows indicate the nematic director. The deformations correspond to director rotations of $\theta = 0°$, 25°, 60°, and 90°. (b) Macroscopic soft deformation in the $x-z$ plane for the thin nematic gel film of $l_x^0/l_z^0 = 40$ and $k = 1.34$ on the basis of eqs 4 and 5. (c) Deformation of the gel with the same parameters as (b) but without body tilting.

an irregular wiggled profile appears in *x*-direction, which precludes us from quantifying the deformation. The deformation of constrained nematic gels ($\gamma_z = 0$) under electric fields was discussed in ref 13, but the constrained condition is different from that in the present study: The distortions in *x*- and *y*-directions at the gel surface are prohibited in their studies,[13] while they are possible here because of the lubrication at the electrode surface. The deformation in the constrained geometry is also an interesting issue, and an alternative method is required to reveal the macroscopic deformations.

Analysis of the Deformation Induced by Director Rotation. In this section, we discuss the relation between the rotation angle of director (θ) and induced deformation. The issue of interest is what the path between the two extreme states at $\theta = 0°$ and $\theta = 90°$ (Figure 5b) is like. Some similarities between our observation and the model of macroscopic soft deformation[1,20,21] are present. The macroscopic soft deformation induced by director rotation consists of pure shear deformation and body rotation,[1,20,21] which is schematically illustrated in part a of Figure 8. The variations of θ from 0° to 90° yield a stretching along the rotated director and a compression along the initial director axis but with no dimensional change in *y*-direction. As stated in the previous section, the experimental results indicate that the real systems are not purely "soft" regarding the energy cost for director rotation. Note the present analysis focuses on the similarities of the experiment and theory in the θ dependence of the deformation. Let us consider the deformation for the thin rectangular nematic gel of the initial lengths l_x^0, l_y^0, and l_z^0 with the initial director along *x*-axis when imposing the electric field in *z*-direction. The theoretical deformation gradient tensor λ for small volume elements (Figure 8a) was derived as[21]

$$\lambda = \begin{pmatrix} 1 - (1 - k^{-1})\sin^2\theta & 0 & (k-1)\sin\theta\cos\theta \\ 0 & 1 & 0 \\ (1 - k^{-1})\sin\theta\cos\theta & 0 & 1 + (k-1)\sin^2\theta \end{pmatrix} \quad (4)$$

where *k* is a measure of shape anisotropy of polymer chains stemming from the nematic order (not from the macroscopic shape of samples). The dimension l_i ($i = x, y, z$) along *i*-axis at $\theta = \theta$ is obtained as

$$l_x = l_x^0\left(\lambda_{xx} + \frac{l_z^0}{l_x^0}\lambda_{xz}\right) \approx l_x^0\lambda_{xx} \quad (5a)$$

$$l_y = l_y^0 \quad (5b)$$

$$l_z = l_z^0\left(\lambda_{zz} + \frac{l_x^0}{l_z^0}\lambda_{zx}\right) \quad (5c)$$

where λ_{ij} ($i, j = x, y, z$) is the *ij* component of λ, and we use the condition $l_z^0 \ll l_x^0$ because l_z^0/l_x^0 of the samples employed is on the order of 10^{-2}. Equation 5a indicates that the contribution of the shear λ_{xz} to Δl_x is negligibly small in sufficiently thin films. Part b of Figure 8 depicts the simulated deformation in the $x-z$ plane for the thin rectangular gel with $l_x^0/l_z^0 = 40$ and $k = 1.34$ on the basis of eqs 4 and 5. In the experiments, the changes in shape are evaluated in terms of γ_i (eq 1). The expression of γ_i using eq 5 is given by

$$\gamma_x = -\left(1 - \frac{1}{k}\right)\sin^2\theta \quad (6a)$$

$$\gamma_y = 0 \quad (6b)$$

$$\gamma_z = (k-1)\sin^2\theta + \frac{l_x^0}{l_z^0}\left(1 - \frac{1}{k}\right)\sin\theta\cos\theta \quad (6c)$$

where $\gamma_i = (l_i - l_i^0)/l_i^0$ ($i = x, y, z$). Most characteristically, the theory predicts γ_x proportional to $\sin^2\theta$ and $\gamma_y = 0$ independent of θ.

In the experiments, $\sin^2\theta$ is obtained from the data of Δn_{eff} using the relation for the systems with uniaxial optical anisotropy ($n_x \geq n_y = n_z$):

$$\sin^2\theta = \frac{{n_{y0}}^2}{{n_{x0}}^2 - {n_{y0}}^2}\left\{\frac{{n_{x0}}^2}{n_x(\theta)^2} - 1\right\} \quad (7)$$

where n_{i0} and $n_i(\theta)$ ($i = x, y$) is the refractive index along *i*-axis at $\theta = 0$ and $\theta = \theta$, respectively, and the uniform orientation is assumed. If $n_{y0} \gg \Delta n_{\text{eff}}$ and $n_{y0} \gg \Delta n_{\text{eff}}^0$, eq 7 is simplified as

$$\sin^2\theta \approx 1 - \frac{\Delta n_{\text{eff}}(\theta)}{\Delta n_{\text{eff}}^0} \quad (8)$$

where $\Delta n_{\text{eff}}^0 = n_{x0} - n_{y0}$. This simplification is valid when the birefringence is sufficiently small relative to the principal refractive indices. Our samples satisfy this condition because Δn_{eff}^0 is on the order of 10^{-2} whereas the refractive index normal to the long axis ($n_\perp$) for 5CB is ca. 1.5 at 25 °C. The values of Δn_{eff}^0 are comparable to those for the side chain LCE with the similar shape anisotropy ($\alpha < 1.5$).[27] Figure 9 illustrates the plots of γ_i ($i = x, y$) vs $\sin^2\theta$ for the gels with varying C_x. For all gels, γ_x linearly varies with $\sin^2\theta$, and $\gamma_y \approx 0$ independently of θ in agreement with eqs 6a and 6b. The values of *k* evaluated from the slope in Figure 9a are tabulated in Table 1. The elasticity theory of nematic rubbers relates the shape anisotropy *k* to a step length anisotropy in anisotropic Gaussian coils in nematic networks.[1,21] In our previous studies,[23,28] it was theoretically shown that the degree of anisotropic swelling α is

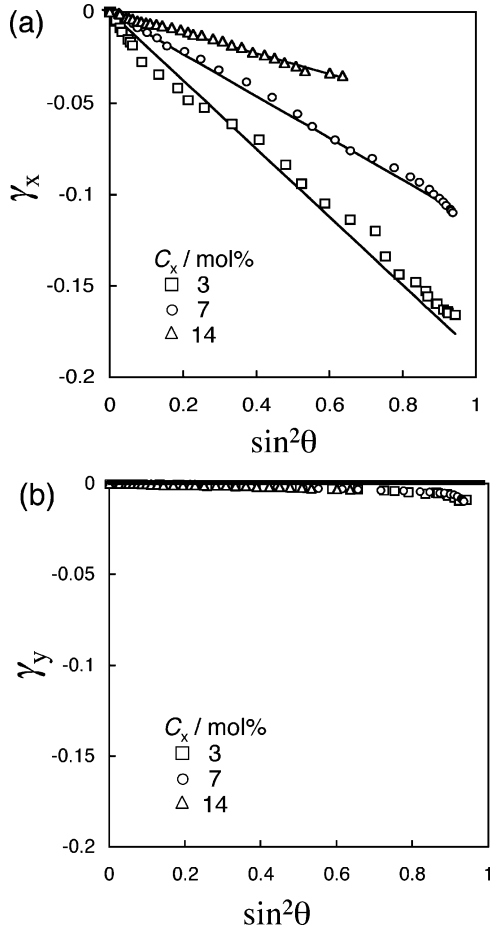

Figure 9. Strains (a) γ_x and (b) γ_y as a function of $\sin^2\theta$ for the nematic gels with differing C_x. The solid lines represent the predictions of eqs 6a and 6b.

equivalent to k. As seen in Table 1, the values of k and α evaluated from the two independent methods are comparable, but the trends for the C_x dependence are opposite. The theory simply expects that the distortion driven by director rotation becomes larger as the shape anisotropy (k) increases, which is clearly seen in Figure 8a. Since the shape anisotropy (obtained from the swelling experiment) increases with C_x, k is theoretically expected to rise with C_x. In opposite to this theoretical expectation, k estimated from the slope in Figure 9 decreases with C_x. A possible reason for the negative C_x dependence of k is the anchoring effect yielding the surface layers where the initial nematic orientation is unaltered or does not change largely even at high fields. The anchoring effect is expected to increase with C_x. When the anchoring effect acting to resist the induced deformation exceeds the shape anisotropy effect, the C_x dependence of k becomes negative as observed in the experiments. Further, C_x alters the degree of swelling (Q) in addition to α, and Q may also influence k, which is not considered in the theory.

A considerable body tilting at $\theta \approx 45°$ expected theoretically (as shown in Figure 8b) is not observed in the experiments. Tangent of body tilt angle ω ($\tan\omega = l_z/l_x$) for sufficiently thin films of $l_z^0 \ll l_x^0$ approximates to $\tan\omega(\theta) \approx \lambda_{zx}/\lambda_{xx} = (1 - k^{-1})\sin\theta\cos\theta/[1 - (1 - k^{-1})\sin^2\theta]$. The tilt angle has the maximum at $\theta \approx 45°$ for the small k (<1.5), whereas ω is zero at $\theta = 0°$ and 90°. As is evident from $\tan\omega_{max} \approx \tan\omega(\theta = 45°) = (k - 1)/(k + 1)$, ω_{max} becomes smaller as k decreases, and the values of k in present study ($1.06 < k < 1.23$) yield ω_{max} ranging from 2° to 6°. Even if ω_{max} is as small as 2°, the material cannot tilt remotely because of the geometric constraints of the electrodes: The resultant $l_z \approx 60\ \mu$m for the material of $l_x = 2$ mm exceeds the gap (<20 μm) between the electrode and sample. The contact of the gels with the transparent electrodes should be easily recognizable in the microscopic observation if it occurs. No appreciable body tilting allows us to estimate the optically effective thickness $d_g(\theta)$ by using $d_g(\theta)/d_g^0 = [(1 + \gamma_x)(1 + \gamma_y)]^{-1}$ mentioned before.

There are several possible reasons for the absence of finite body tilting. The first is the effects of rigid surface layer (stemming mainly from anchoring effect) and/or surface tension suppressing the variation of the outline of gels caused by the director reorientation. The excellent agreements of the θ dependence of γ_x and γ_y in the experiment and theory, however, suggest that even if the materials have the rigid surface layers, the inner matrix occupying most part of the materials (excepting the rigid surface layers) deforms in the similar way to the soft deformation, and the macroscopic distortions are governed by the deformation of the inner gel matrix. An appreciable body tilting expected theoretically would arise when the gels have a flexible surface which distorts reflecting the nematogen realignment. The second is that the geometric constraint of the electrodes may yield a counter rotation canceling a net tilting. The counter rotation also affects the rotation angle of director (θ) and the apparent length (l_x) if it occurs, but the influences would not be very noticeable because ω_{max} is small ($\omega_{max} < 6°$). The similar θ dependence of γ_x would be observed even if the body tilting is canceled by counter rotation throughout the process of director rotation. Experiments using samples with cubic shape and large k will be needed to discuss the issue of body tilting unambiguously. The deformation along these scenarios is schematically shown in Figure 8c.

Summary

The sufficiently high electric fields achieve almost full realignment of the director in unconstrained nematic gels along the field axis. The director switching yields the simultaneous deformation occurring in the plane where the director rotates. The compressive strain along the initial director axis grows in proportion to the square of $\sin\theta$ where θ is the rotation angle, while appreciable dimensional variation is absent in the direction irrelevant to the director rotation. The θ dependence of the strains agrees well with the theoretical prediction of macroscopic soft deformation for thin films, although the accompanying appreciable body tilting expected by the theory is not observed in the experiments. The mechanical constraint prohibiting strain along the field axis significantly suppresses the director reorientation and the resulting deformation.

Acknowledgment. The authors appreciate helpful comments from Prof. E. M. Terentjev and a referee. The authors thank Nissan Chemical Industries and Chiba Specialty Chemicals Co. for the provisions of the polyimide solution and photoinitiator, respectively. This work was partly supported by a grant from the Murata Science Foundation, a Grant-in-Aid (No. 16750186), and the 21st century COE program "COE for a United Approach to New Materials Science" from the Ministry of Education, Culture, Sports, Science, and Technology, Japan.

References and Notes

(1) Warner, M.; Terentjev, E. M. *Liquid Crystal Elastomers*; Oxford University Press: Oxford, 2003.
(2) Mitchell, G. R.; Davis, F. J.; Guo, W. *Phys. Rev. Lett.* **1993**, *71*, 2947.
(3) Kundler, I.; Finkelmann, H. *Macromol. Chem. Rapid Commun.* **1995**, *16*, 679.

(4) Finkelmann, H.; Kundler, I.; Terentjev, E. M.; Warner, M. *J. Phys. II* **1997**, *7*, 1059.
(5) Roberts, P. M.; Mitchell, G. R.; Davis, F. J. *J. Phys. II* **1997**, *7*, 1337.
(6) Zubarev, E. R.; Kupstov, S. A.; Yuranova, T. I.; Talroze, R. V.; Finkelmann, H. *Liq. Cryst.* **1999**, *26*, 1531.
(7) Conti, S.; DeSimone, A. *Phys. Rev. E* **2002**, *66*, 061710.
(8) Zentel, R. *Liq. Cryst.* **1986**, *1*, 589.
(9) Barnes, N. R.; Davis, F. J.; Mitchell, G. R. *Mol. Cryst. Liq. Cryst.* **1989**, *168*, 13.
(10) Kishi, R.; Kitano, T.; Ichijo, H. *Mol. Cryst. Liq. Cryst.* **1996**, *280*, 109.
(11) Hikmet, R. A. M.; Boots, H. M. J. *Phys. Rev. E* **1997**, *51*, 5824.
(12) Chang, C.-C.; Chien, L.-C.; Meyer, R. B. *Phys. Rev. E* **1997**, *56*, 595.
(13) Terentjev, E. M.; Warner, M.; Meyer, R. B.; Yamamoto, J. *Phys. Rev. B* **1999**, *60*, 1872.
(14) Ren H.; Wu, S. T. *Appl. Phys. Lett.* **2002**, *81*, 1432.
(15) Huang, C.; Zhang, Q.; Jákli, A. *Adv. Funct. Mater.* **2003**, *13*, 525.
(16) Kempe, M. D.; Scruggs, N. R.; Verduzco, R.; Lal, J.; Kornfield, J. A. *Nat. Mater.* **2004**, *3*, 177.
(17) Urayama, K.; Kondo, H.; Arai, Y. O.; Takigawa, T. *Phys. Rev. E* **2005**, *71*, 051713.
(18) Urayama, K.; Honda, S.; Takigawa, T. *Macromolecules* **2005**, *38*, 3574.
(19) Yusuf, Y.; Huh, J.-H.; Cladis, P, E.; Brand, H. R.; Finkelmann, H.; Kai, S. *Phys. Rev. E* **2005**, *71*, 061702.
(20) Olmsted, P. D. *J. Phys. II* **1994**, *4*, 2215.
(21) Verwey, G. C.; Warner, M. *Macromolecules* **1995**, *28*, 4303.
(22) Calvert, P. In *Electroactive Polymer (EAP) Actuators as Artificial Muscles—Reality, Potential, and Challenges*; Bar-Cohen, Y., Ed.; SPIE: Bellingham, WA, 2001.
(23) Urayama, K.; Arai, Y. O.; Takigawa, T. *Macromolecules* **2005**, *38*, 3469.
(24) Terentjev, E. M.; Warner, M.; Bladon, H. *J. Phys. II* **1994**, *4*, 667.
(25) Warner, M.; Bladon, P.; Terentjev, T. M. *J. Phys. II* **1994**, *4*, 91.
(26) Golubovic, L.; Lubensky, T. C. *Phys. Rev. Lett.* **1989**, *63*, 1082.
(27) Finkelmann, H.; Greve, A.; Warner, M. *Eur. Phys. J. E* **2001**, *5*, 281.
(28) Urayama, K.; Arai, Y. O.; Takigawa, T. *Macromolecules* **2005**, *38*, 5721.

MA052762Q